The Astrophysical Journal, 864:121 (15pp), 2018 September 10 https://doi.org/10.3847/1538-4357/aad696

High-resolution Spectroscopy of the Relatively Hydrogen-poor Metal-rich Giants in the Globular Cluster ω Centauri

B. P. Hema[1], Gajendra Pandey[1], and R. Srianand[2]
[1] Indian Institute of Astrophysics, Koramangala II Block, Bengaluru, Karnataka, 560034, India; hema@iiap.res.in
[2] Inter-University Centre for Astronomy and Astrophysics, Post Bag 4, Ganeshkhind, Pune 411007, India
Received 2018 May 31; revised 2018 July 27; accepted 2018 July 27; published 2018 September 5

Abstract

High-resolution optical spectra are analyzed for two of the four metal-rich, mildly hydrogen-poor or helium-enhanced giants discovered by Hema & Pandey, along with their comparison normal (hydrogen-rich) giants. The strengths of the MgH bands in the spectra of the program stars are analyzed for their derived stellar parameters. The observed spectra of the sample (hydrogen-poor) stars (LEID 39048 and LEID 34225) show weaker MgH bands, unlike in the spectra of the normal comparison giants (LEID 61067 and LEID 32169). The magnesium abundance derived from MgH bands is less by 0.3 dex or more for LEID 39048 and LEID 34225 than that derived from Mg I lines. This difference cannot be reconciled by making the changes to the stellar parameters within the uncertainties. This difference in the magnesium abundances derived from Mg I lines and from the MgH band is unacceptable. This difference is attributed to the hydrogen deficiency or helium enhancement in their atmospheres. These metal-rich, hydrogen-poor or helium-rich giants provide an important link to the evolution of the metal-rich subpopulation of ω Cen. These stars provide the first direct spectroscopic evidence for the presence of the He enhancement in the metal-rich giants of ω Cen.

Key words: globular clusters: individual (Omega Centauri) – stars: abundances – stars: chemically peculiar

1. Introduction

The brightest and most massive Galactic globular cluster (GGC), ω Cen, exhibits a large spread in metallicity ([Fe/H]) and other abundance anomalies among the cluster stars (Bedin et al. 2004; Sollima et al. 2005; Johnson & Pilachowski 2010; Simpson & Cottrell 2013), including the existence of multiple stellar populations with the cluster dwarfs/giants having normal helium and enhanced helium or relatively hydrogen-poor (H-poor) atmospheres (Piotto et al. 2005; Villanova et al. 2007; Dupree & Avrett 2013).

The doubt is as follows: these relatively H-poor or He-rich giants may be appearing more metal-rich than they really are, due to the lower continuum absorption. Note that the spectra of H-poor F- and G-type supergiants, R Coronae Borealis (RCB) stars, and H-deficient carbon (HdC) stars appear metal-rich when compared with the spectra of normal F- and G-type supergiants (Pandey et al. 2004). This is ascribed to the lower continuum opacity in the atmosphere due to H deficiency. Hence, these stars appear more metal-rich than they actually are (Sumangala Rao et al. 2011). The origin and evolution of these enigmatic stars, RCB/HdC, are not yet clear owing to their rarity and chemical peculiarity.

A low-resolution optical spectroscopic survey was conducted among the giants of ω Cen for identifying new RCB stars (Hema & Pandey 2014). Identifying RCB stars in a globular cluster gives an idea of their position on the H-R diagram and is a potential clue to understanding their origin and evolution.

The Hema & Pandey (2014) survey resulted in the discovery of four mildly H-deficient giants in ω Cen. For two out of these four giants, high-resolution spectra were obtained along with their comparison stars with similar stellar parameters to these two giants. In this paper we have conducted a detailed high-resolution spectroscopic analysis for two mildly H-deficient giants along with their comparison stars to confirm their H deficiency or the He enhancement. The color–magnitude diagram for our program stars and for the sample red giants of Johnson & Pilachowski (2010) is given in Figure 1.

2. Observations and Data Reduction

The high-resolution optical spectra were obtained using the Southern African Large Telescope (SALT) high-resolution spectrograph (HRS).[3] These spectra obtained with SALT-HRS have a resolving power R ($\lambda/\Delta\lambda$) of 40,000. The spectra were obtained with both blue and red cameras using 2K × 4K and 4K × 4K CCDs, respectively, spanning a spectral range of 370–550 nm in the blue and 550–890 nm in the red.

The spectral reductions were carried out using the IRAF software. The traditional data reduction procedure, including bias subtraction, flat-field correction, spectrum extraction, wavelength calibration, etc., was followed.

The extracted and wavelength-calibrated 1D spectra were continuum normalized. The region of the spectrum with maximum flux points and free of absorption lines was considered for continuum fitting with a smooth curve passing through these points. To improve the signal-to-noise ratio, the observed spectra of the program stars were smoothed such that the strengths of the spectral lines are not altered. The signal-to-noise ratio per pixel is ∼150 for the smoothed blue spectra of the program stars at about 5000 Å and ∼200 for red spectra at about 7000 Å. Since there is an overlap of wavelengths, the spectrum is continuous without gaps in the blue and red spectral range. The atlas of high-resolution spectra of Arcturus (Hinkle et al. 2000) was used as a reference for continuum fitting and also for identifying the spectral lines.

[3] SALT-HRS is a dual-beam, fiber-fed, white-pupil, echelle spectrograph, employing VPH gratings as cross dispersers.

Table 1
Photometric and Spectroscopic Parameters for the Program Stars

Parameters	LEID 34225	LEID 39048	LEID 61067	LEID 32169
RA (J2000)	13 27 53.7	13 26 3.9	13 26 50.7	13 27 33.2
Decl (J2000)	−47 24 43.3	−47 26 54.1	−47 37 1.0	−47 23 47.9
M_v (mag)	13.0	12.8	12.5	13.3
$B - V$	1.23	1.42	1.60	1.17
Metallicity ([Fe/H])	−1.0	−0.65	−1.0	−1.0
$V_{\rm helio}$ (km/s)	235 ± 0.5	238 ± 0.5	230 ± 0.5	230 ± 0.5
Date of observation	2016 May 27	2016 May 3	2016 May 15	2016 Jun 25
$T_{\rm eff}$ (K)[a]	4275 ± 50	3965 ± 50	4040 ± 50	4285 ± 50
log g (cgs units)[a]	1.30 ± 0.1	0.95 ± 0.1	0.85 ± 0.1	1.35 ± 0.1
ξ_t (km/s)[a]	1.6 ± 0.1	1.6 ± 0.1	1.6 ± 0.1	1.6 ± 0.1
$T_{\rm eff}$ (K)[b]	4265 ± 50	3965 ± 50	4035 ± 50	4285 ± 50
log g (cgs units)[b]	1.30 ± 0.15	0.95 ± 0.15	0.85 ± 0.15	1.35 ± 0.15
ξ_t (km/s)[b]	1.6 ± 0.2	1.6 ± 0.2	1.6 ± 0.2	1.6 ± 0.2
$T_{\rm eff}$ (K)[c]	4266 ± 50	3945 ± 50	4010 ± 50	4260 ± 50
log g (cgs units)[c]	1.35 ± 0.1	1.0 ± 0.1	0.95 ± 0.1	1.4 ± 0.1

Notes.
[a] This work.
[b] From Johnson & Pilachowski (2010).
[c] Photometric determinations from Hema & Pandey (2014).

3. Abundance Analysis

In order to conduct a detailed abundance analysis, the equivalent widths for weak and strong lines of several elements that are clean and also not severely blended for both neutral and ionized states were measured using different commands in IRAF.

The wavelength-calibrated spectrum of a program star (LEID 39048) was used to measure the shift of the spectral lines from the rest wavelengths; the Hinkle et al. (2000) atlas of Arcturus was used as a reference. Adopting LEID 39048's spectrum as a template, the radial velocities and the uncertainties involved were determined for other program stars using the task *fxcor* in IRAF. Then, the heliocentric corrections were applied to these radial velocities. The heliocentric velocities for the program stars are given in Table 1 and are in good agreement with the mean velocity of the cluster, $V_r = 233\,{\rm km\,s^{-1}}$, with the dispersion ranging from 15 to $6\,{\rm km\,s^{-1}}$ from the center outward, respectively (Mayor et al. 1997).

For the determination of stellar parameters and the elemental abundances, the LTE line analysis and spectrum synthesis code MOOG (Sneden 1973) and the ATLAS9 (Kurucz 1998) plane-parallel, line-blanketed LTE model atmospheres were used.

The microturbulence (ξ_t) is derived using Fe I lines having a similar excitation potential and a range in equivalent width, weak to strong, giving the same abundance. The effective temperature ($T_{\rm eff}$) is determined using the excitation balance of Fe I lines having a range in lower excitation potential. The $T_{\rm eff}$ and ξ_t were fixed iteratively. The process was carried out until both returned zero slope.

By adopting the determined $T_{\rm eff}$ and ξ_t, the surface gravity (log g) is derived. The surface gravity is fixed by demanding the same abundances from the lines of different ionization states of a species, known as ionization balance. The surface gravity is derived using the lines of Fe I/Fe II, Ti I/Ti II, and Sc I/Sc II. Then, the mean log g was adopted.

Uncertainty on the $T_{\rm eff}$ and ξ_t is estimated by changing the $T_{\rm eff}$ in steps of 25 K and ξ_t in steps of $0.05\,{\rm km\,s^{-1}}$. The change in $T_{\rm eff}$ and ξ_t and the corresponding deviations in abundance, from the zero slope abundance, of about 1σ error, is obtained. This change is adopted as the uncertainty on these parameters. The adopted $\Delta T_{\rm eff} = \pm 50\,{\rm K}$ and $\Delta\xi_t = \pm 0.1\,{\rm km\,s^{-1}}$ (see Figure 2). The uncertainty on log g is the standard deviation from the mean value of the log g determined from different species, which is about ±0.1 (cgs units). The adopted stellar parameters with the uncertainties are given in Table 1.

The log g values for the program stars in Hema & Pandey (2014) were derived using the standard relation:

$$\log(g_*) = 0.40(M_{\rm bol.} - M_{\rm bol,\odot}) + \log(g_\odot) + 4(\log(T/T_\odot)) + \log(M/M_\odot). \quad (1)$$

The bolometric correction to M_v was applied using the relation given by Alonso et al. (1999). The distance modulus for ω Cen is $(m - M)_v = 13.7$, and the mass of ω Cen red giants was assumed to be $0.8\,M_\odot$ (Johnson & Pilachowski 2010). Using the photometric temperatures derived from $(J - H)_0$, $(J - K)_0$, and $(b - y)$ colors in Equation (1), the log g values were derived.

The difference in the log g values derived by us and those derived by Johnson & Pilachowski (2010) is within ±0.1 (cgs units). Hence, the uncertainty on the log g values adopted by Hema & Pandey (2014) was about ±0.1 (cgs units; for details see Hema & Pandey 2014).

Figure 3 shows the ($T_{\rm eff}$, log g) plane for the program stars LEID 34225, LEID 61067, and LEID 32169. For LEID 39048, no lines from ionized states were available. Hence, the log g values determined from photometric estimates from our previous study (Hema & Pandey 2014) were adopted. The log g values derived by Hema & Pandey (2014) and Johnson & Pilachowski (2010) are in excellent agreement. The uncertainties on the ($T_{\rm eff}$, log g) for the program stars derived by Johnson & Pilachowski (2010) are about ±50 K and ±0.15 (cgs), respectively, and those derived photometrically by Hema & Pandey (2014) are about ±100 K and ±0.1 (cgs), respectively, which are in fair agreement.

For abundance analyses, the line list of Johnson & Pilachowski (2010) was used. The elements for which the

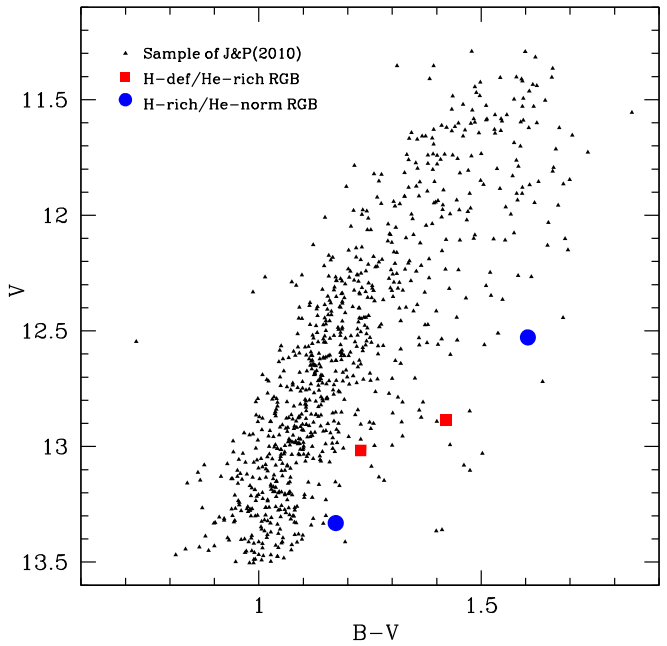

Figure 1. Color–magnitude diagram for our sample ω Cen red giants along with the sample red giants from Johnson & Pilachowski (2010). All the photometric data are from Johnson & Pilachowski (2010). The filled red squares are the H-deficient/He-enhanced giants, and the filled blue circles are the normal giants of our sample. The filled black triangles are the sample red giants of Johnson & Pilachowski (2010).

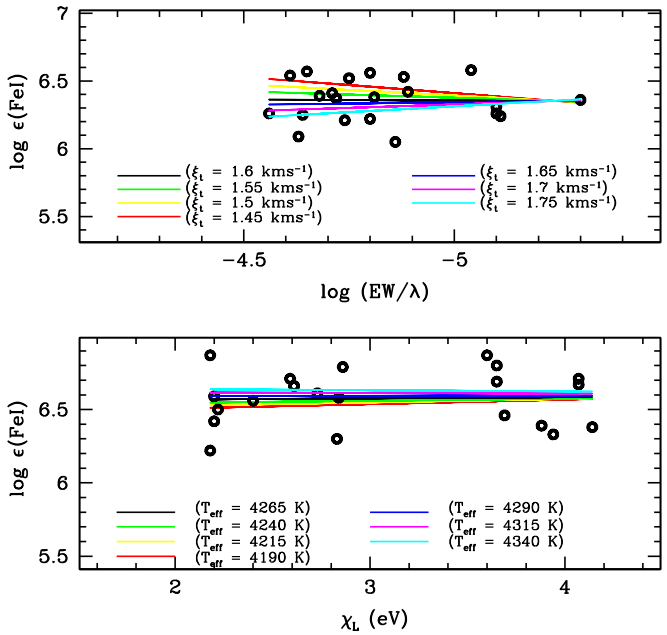

Figure 2. Estimation of uncertainties on $T_{\rm eff}$ (bottom panel) and ξ_t (top panel). The adopted stellar parameters for deriving $\Delta T_{\rm eff}$ and $\Delta\xi_t$ are ($T_{\rm eff}$, log g, ξ_t) = (4265 K, 1.3 cgs units, 1.6 km s^{-1}). The adopted uncertainties corresponding to the 1σ error on the abundance of the zero slope are $\Delta T_{\rm eff} = \pm 50$ K and $\Delta\xi_t = 0.1$ km s^{-1}.

lines are very few or none in the Johnson & Pilachowski (2010) list were adopted from Ramírez & Allende Prieto (2011). However, to cross-examine, the stellar parameters and the Fe abundances were also derived from the Fe I and Fe II lines of Ramírez & Allende Prieto (2011) for one of the program stars, i.e., LEID 34225. These derived parameters are in line with those determined from the Fe I and Fe II lines of Johnson & Pilachowski (2010). The line list used for the determination of the stellar parameters and the abundances for the program stars are given in Table 2. The Fe I and Fe II lines of Ramírez & Allende Prieto (2011) for LEID 34225 are given in Table 3. Table 4 gives the abundance ratios ([E/Fe]) for different elements of the program stars. The adopted solar abundances from Asplund et al. (2009) are also given. The typical errors on elemental abundances due to the uncertainties on the stellar parameters and the signal-to-noise ratio are given in Table 5. The rms error due to these parameters is given along with the standard deviation in the abundances due to line-to-line scatter in the last two columns of Table 5. An Mg I line at 5711 Å in our program stars is also synthesized to support the Mg abundance derived from the Mg I equivalent width analysis (see Figure 4).

4. MgH Band and the Spectrum Syntheses

In our previous study (Hema & Pandey 2014), the low-resolution optical spectra of the globular cluster ω Cen giants were analyzed to identify the H-deficient stars by examining the strengths of the Mg b atomic lines and the blue degraded (0,0) MgH band. Based on the strengths of these features, the observed program stars were divided into three groups: (1) metal-rich giants with strong Mg b lines and also the MgH band, (2) metal-poor giants with no Mg b line and no MgH band, and (3) metal-rich giants with strong Mg b lines and weak/no MgH band, in their observed spectra. The Hema & Pandey (2014) analysis, which included comparison of stars' spectra with similar stellar parameters and spectrum synthesis of the MgH band for the star's adopted stellar parameters, resulted in identification of four mildly H-deficient stars: two from the first group (LEID 39048 and LEID 60073) and two from the third group (LEID 34225 and LEID 193804).

High-resolution spectra of two stars, LEID 39048 (a first-group star) and LEID 34225 (a third-group star), including two comparison stars, were obtained from SALT for confirming their H deficiency. For example, the SALT spectrum of LEID 34225 is superposed on the SALT spectrum of a comparison star, LEID 32169 (see Figure 5); note that these stars have similar stellar parameters, i.e., effective temperature, surface gravity, and metallicity. As discussed in Hema & Pandey (2014), the strengths of MgH bands in the observed spectra of LEID 39048 and LEID 34225 are weaker than that expected for their derived stellar parameters. To validate our continuum fitting in the MgH band region, we measured the equivalent width for the Fe I lines in this region and derived the abundances. The derived abundances are in excellent agreement with those derived from the other wavelength regions.

For their derived stellar parameters, the spectra of these stars were synthesized in the window 5170–5190 Å to examine the strengths of Mg b lines and the MgH bands in their observed spectra carefully. The spectrum synthesis for the program stars was carried out following the procedure explained in Hema & Pandey (2014). The LTE spectrum synthesis code synth in MOOG, combined with the ATLAS9 (Kurucz 1998) plane-parallel and line-blanketed LTE model atmospheres, was used to synthesize the spectra of our program stars. The molecular and the atomic line lists, both validated by synthesizing the high-resolution spectrum of Arcturus provided by Hinkle et al. (2000), were adopted for synthesis. The Mg isotopic ratio,

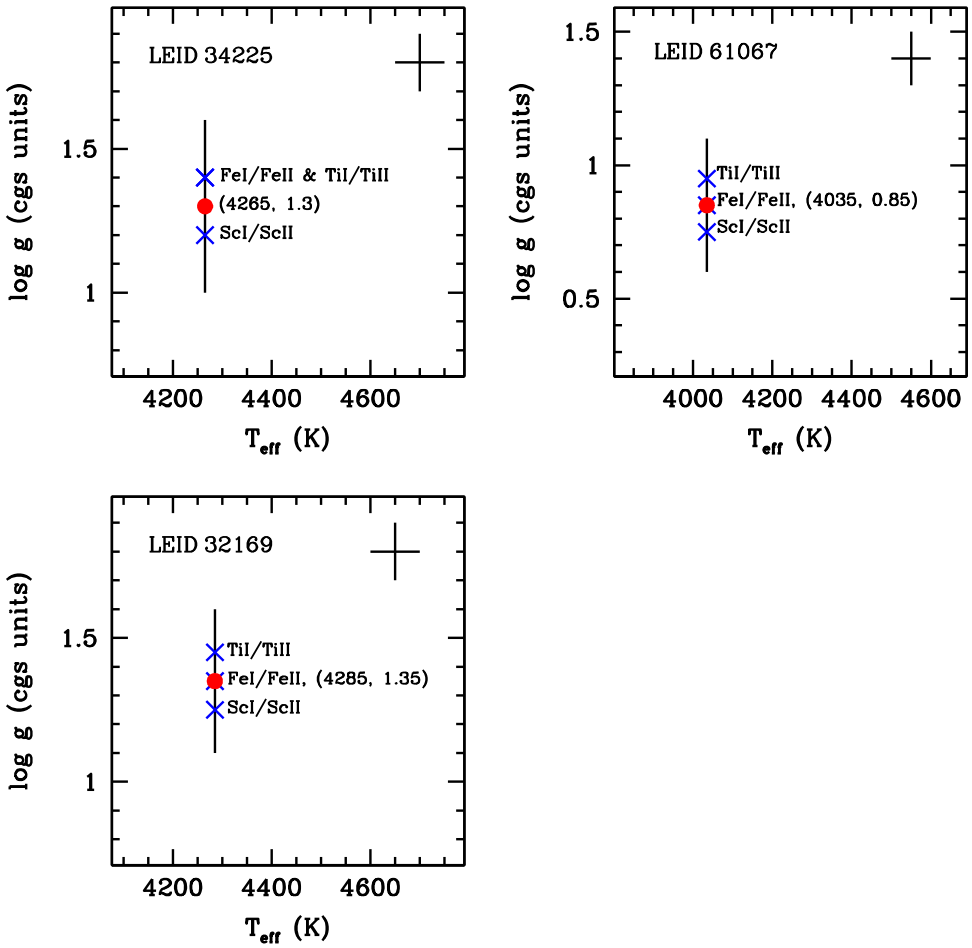

Figure 3. Plane of $T_{\rm eff}$ and log g for LEID 34225, LEID 61067, and LEID 32169. The vertical line shows the excitation balance from Fe I lines. The blue crosses on the vertical line are the log g values derived from the ionization balance of Fe I/Fe II, Sc I/Sc II, and Ti I/Ti II. The mean/adopted ($T_{\rm eff}$, log g) is shown with a red circle. The error bars on $T_{\rm eff}$ and log g are shown in the upper right corner.

^{24}Mg:^{25}Mg:^{26}Mg = 82:09:09, was adopted for Arcturus from McWilliam & Lambert (1988). The synthesized spectrum was convolved with a Gaussian profile with a width that represents the instrumental broadening, as the effects due to macro-turbulence and the rotational velocity are very small or negligible.

The spectra were synthesized in the wavelength window from 5170 to 5190 Å. The observed spectrum bluer than 5170 Å falls at the edge of the order. Our examination of the observed spectra shows very strong saturated Mg *b* lines at 5167.3, 5172.68, and 5183.6 Å; The subordinate lines of the MgH band are blended with these strong Mg *b* lines. Hence, the subordinate lines in the wavelength region 5175–5176 Å, where there are pure molecular lines, were given more weight. However, a fit to these MgH features gives an overall best fit to the whole range of the MgH band spanning from about 5160 to 5190 Å. The mean of the isotopic ratios derived for the red giants of ω Cen by Da Costa et al. (2013), which is about ^{24}Mg:^{25}Mg:^{26}Mg = 70:13:15, with the uncertainty on each value being about ±4, was adopted for our program stars, providing a fairly good fit throughout the span of the MgH band. Note that the Mg *b* lines are very strong and are saturated in the spectra of our program stars, and hence these lines are not used for estimating the Mg abundance from the Mg I line or MgH band. The weaker atomic Mg I lines are used for deriving the Mg I abundance (those given in Table 2), and the Mg abundance from the MgH band is derived using pure MgH molecular lines that are not blended with the strong Mg *b* lines.

The spectra of the program stars were synthesized using their derived stellar parameters and the elemental abundances as discussed in Section 3. The syntheses of the spectra for the individual program stars are discussed below.

LEID 32169: this is a first-group star, which is relatively metal-rich, having strong Mg *b* lines and a strong MgH band. This is a comparison for the first-group mildly H-deficient stars and here for the sample star, LEID 34225. The spectrum of LEID 32169 shows a well-represented MgH band. Using its derived stellar parameters, ($T_{\rm eff}$, log g, ξ_t, [Fe/H]) = (4285 ± 50, 1.35 ± 0.1, 1.6 ± 0.1, −1.0), the MgH band is synthesized by varying the Mg abundance to obtain the best fit for the observed spectrum (see Figure 6). The MgH band synthesized for the log ϵ(Mg) = 6.8 dex ([Mg/Fe] = +0.26) provides the best fit to the observed spectrum, and this is in excellent agreement with the Mg abundance derived from Mg I lines. The Mg abundance derived from the MgH band is as expected for the star's metallicity and also that derived from the Mg I lines.

LEID 61067: This is a first-group star, which is relatively metal-rich, having strong Mg *b* lines and a strong MgH band. This is a comparison for the third-group sample star LEID 39048. The observed spectrum shows the well-represented MgH

Table 2
Line List Used for the Abundance Analysis of the Program Stars

Wavelength (Å)	χ(eV) (eV)	log gf	LEID 34225 (mÅ)/log $\epsilon(E)$[a]	LEID 39048 (mÅ)/log $\epsilon(E)$[a]	LEID 61067 (mÅ)/log $\epsilon(E)$[a]	LEID 32169 (mÅ)/log $\epsilon(E)$[a]
O I λ6300.31	0.00	−9.75	13/7.40	43/8.06	33/5.65	21/7.71
O I λ6363.78	0.02	−10.19	⋯	21/8.15	⋯	10/7.81
Mean (log ϵ(O I))	⋯	⋯	7.4	8.1 ± 0.06	7.73	7.76 ± 0.07
Na I λ4751.82[b]	2.10	−2.08	26/5.73	⋯	79/6.46	34/5.91
Na I λ5148.84[b]	2.10	−2.04	39.7/5.93	⋯	76/6.31	41/5.96
Na I λ6154.23	2.10	−1.57	58/5.67	134/6.53	122/6.42	79/6.00
Na I λ6160.75	2.10	−1.27	70/5.55	149/6.47	142/6.44	98/5.97
Mean (log ϵ(Na I))	⋯	⋯	5.72 ± 0.16	6.50 ± 0.04	6.40 ± 0.07	5.96 ± 0.04
Mg I λ4730.04[b]	4.34	−2.39	⋯	97/7.27	89/7.10	⋯
Mg I λ5711.09[b]	4.34	−1.73	105/6.70	145/7.35	121/6.86	115/6.88
Mg I λ6318.72[b]	5.11	−1.73	40/6.60	83/7.52	69/7.01	39/6.61
Mg I λ6319.24[b]	5.11	−1.95	29/6.61	49/7.43	56/7.01	34/6.74
Mg I λ7657.61[b]	5.11	−1.28	78/6.70	126/7.47	106/7.05	85/6.81
Mean (log ϵ(Mg I))	⋯	⋯	6.65 ± 0.05	7.41 ± 0.1	7.00 ± 0.1	6.80 ± 0.14
Al I λ6696.03	3.14	−1.57	100/6.37	119/6.37	110/6.30	79/6.05
Al I λ6698.67	3.14	−1.89	89/6.49	103/6.42	90/6.30	66/6.14
Al I λ7835.31	4.02	−0.64	93/6.66	99/6.56	73/6.23	59/6.15
Al I λ7836.13	4.02	−0.49	91/6.47	115/6.65	108/6.59	75/6.24
Mean (log ϵ(Al I))	⋯	⋯	6.50 ± 0.12	6.50 ± 0.13	6.35 ± 0.16	6.15 ± 0.08
Si I λ5684.48[b]	4.95	−1.65	58/6.91	71/7.45	59/7.01	48/6.76
Si I λ5690.42[b]	4.93	−1.87	47/6.92	50/7.22	67/7.35	50/6.98
Si I λ5701.10[b]	4.93	−2.05	48/7.11	40/7.19	41/7.03	31/6.79
Si I λ5772.15[b]	5.08	−1.75	57/7.16	62/7.54	58/7.28	46/6.97
Si Iλ5793.07[b]	4.93	−2.06	41/6.97	56/7.52	54/7.29	⋯
Si I λ6155.13	5.62	−0.78	⋯	75/7.20	81/7.08	66/6.68
Si I λ6237.32	5.61	−1.28	⋯	80/7.41	74/7.07	69/6.85
Mean (log ϵ(Si I))	⋯	⋯	7.00 ± 0.11	7.36 ± 0.15	7.16 ± 0.14	6.84 ± 0.12
Ca I λ5260.39[b]	2.52	−1.90	50/5.59	⋯	78/5.82	57/5.73
Ca I λ5867.56[b]	2.93	−0.80	60/5.17	⋯	89/5.42	89/5.68
Ca I λ6161.29	2.52	−1.28	83/5.20	143/5.85	140/5.89	98/5.47
Ca I λ6162.18	1.90	−0.07	⋯	345/5.88	295/5.58	233/5.41
Ca I λ6166.44	2.52	−1.11	96/5.31	158/6.00	135/5.69	106/5.49
Ca I λ6169.04	2.52	−0.69	122/5.43	168/5.80	146/5.53	125/5.47
Ca I λ6169.56	2.53	−0.27	135/5.39	191/5.85	171/5.66	142/5.50
Ca I λ6455.60[b]	2.52	−1.34	90/5.62	137/6.01	111/5.66	95/5.70
Ca I λ6471.66[b]	2.53	−0.59	126/5.50	172/5.84	151/5.59	136/5.67
Ca I λ6499.65[b]	2.52	−0.59	124/5.45	176/5.88	⋯	134/5.61
Mean (log ϵ(Ca I))	⋯	⋯	5.40 ± 0.16	5.9 ± 0.08	5.65 ± 0.14	5.57 ± 0.12
Sc I λ4743.82[b]	1.45	0.07	⋯	⋯	91/2.34	⋯
Sc I λ5081.56[b]	1.45	0.06	⋯	⋯	79/2.10	⋯
Sc I λ5484.63[b]	1.85	0.08	20/2.47	⋯	32/2.38	⋯
Sc I λ5671.83[b]	1.45	0.64	69/2.22	⋯	101/2.32	59/2.08
Sc I λ6210.67	0.00	−1.53	58/2.08	⋯	100/2.05	69/2.27
Sc I λ6305.66	0.02	−1.30	85/2.17	⋯	138/2.36	67/1.97
Mean (log ϵ(Sc I))	⋯	⋯	2.24 ± 0.16	⋯	2.26 ± 0.14	2.10 ± 0.15
Sc II λ5357.20[b]	1.51	−2.21	19/2.36	⋯	17/2.21	18/2.38
Sc II λ5552.23[b]	1.46	−2.28	⋯	⋯	32/2.57	18/2.36
Sc II λ5684.21[b]	1.51	−1.07	74/2.29	69/2.28	72/2.16	56/2.00
Sc II λ6245.62	1.51	−0.98	80/2.27	95/2.60	86/2.25	60/1.97
Sc IIλ6300.75	1.51	−1.84	29/2.19	49/2.67	35/2.23	31/2.28
Sc II λ6320.84	1.50	−1.77	30/2.14	45/2.51	38/2.19	⋯
Sc II λ6604.58	1.36	−1.48	⋯	96/2.85	79/2.39	⋯
Mean (log ϵ(Sc II))	⋯	⋯	2.25 ± 0.09	2.60 ± 0.2	2.28 ± 0.14	2.20 ± 0.2
Ti I λ5219.70[b]	0.02	−2.29	140/4.49	200/4.93	185/4.84	⋯
Ti I λ5295.77[b]	1.07	−1.63	93/4.44	141/4.82	120/4.47	78/4.18
Ti I λ5490.15[b]	1.46	−0.93	99/4.38	⋯	129/4.48	87/4.17
Ti I λ5702.66[b]	2.30	−0.44	⋯	99/4.54	67/4.10	31/3.86
Ti I λ5716.44[b]	2.30	−0.72	34/4.20	86/4.59	70/4.44	30/4.15
Ti I λ6092.79[b]	1.89	−1.32	⋯	⋯	56/4.18	25/4.06
Ti I λ6146.23	1.87	−1.51	⋯	⋯	70/4.17	22/3.78
Ti I λ6258.11	1.44	−0.38	⋯	197/4.75	161/4.20	105/3.74

Table 2
(Continued)

Wavelength (Å)	χ(eV) (eV)	log gf	LEID 34225 (mÅ)/log $\epsilon(E)$[a]	LEID 39048 (mÅ)/log $\epsilon(E)$[a]	LEID 61067 (mÅ)/log $\epsilon(E)$[a]	LEID 32169 (mÅ)/log $\epsilon(E)$[a]
Ti I λ6261.10	1.43	−0.49	⋯	210/5.05	169/4.46	104/3.82
Ti I λ6303.76	1.44	−1.69	58/4.19	145/5.03	95/4.27	56/4.19
Ti I λ6312.24	1.46	−1.55	⋯	139/4.94	93/4.25	37/3.90
Ti I λ6336.11	1.44	−1.69	⋯	126/4.85	81/4.25	30/3.94
Ti I λ6599.10[b]	0.90	−2.08	73/4.12	155/4.77	133/4.47	69/4.09
Ti I λ7357.73[b]	1.44	−1.12	98/4.22	166/4.65	169/4.77	⋯
Ti I λ8675.37[b]	1.07	−1.67	⋯	⋯	162/4.29	100/4.09
Ti I λ8682.98[b]	1.05	−1.94	⋯	⋯	149/4.37	66/3.94
Ti I λ8734.71[b]	1.05	−2.38	⋯	⋯	138/4.66	⋯
Mean (log ϵ(Ti I))	⋯	⋯	4.30 ± 0.14	4.80 ± 0.17	4.40 ± 0.2	4.0 ± 0.16
Ti II λ4583.41[b]	1.17	−2.72	87/4.33	⋯	99/4.52	⋯
Ti II λ4708.66[b]	1.24	−2.21	111/4.43	⋯	⋯	90/3.98
Ti II λ5336.78[b]	1.58	−1.70	113/4.25	⋯	121/4.34	107/4.16
Ti II λ5418.77[b]	1.58	−1.99	95/4.16	⋯	109/4.37	81/3.91
Mean (log ϵ(Ti II))	⋯	⋯	4.29 ± 0.11	⋯	4.40 ± 0.1	4.02 ± 0.13
V I λ6039.73[b]	1.06	−0.65	⋯	125/3.26	113/3.13	54/2.73
V I λ6081.44[b]	1.05	−0.58	66/2.81	137/3.39	124/3.23	63/2.78
V I λ6090.21[b]	1.08	−0.06	74/2.44	149/3.15	132/2.90	87/2.65
V I λ6119.53[b]	1.06	−0.32	72/2.63	131/3.02	118/2.86	89/2.92
V I λ6135.36[b]	1.05	−0.75	41/2.58	122/3.25	102/3.02	56/2.84
V I λ6274.65[b]	0.27	−1.67	⋯	139/3.18	129/3.08	73/2.84
V I λ6285.16[b]	0.28	−1.51	81/2.77	154/3.33	⋯	73/2.84
V I λ6531.41[b]	1.22	−0.84	31/2.71	86/2.97	79/2.98	47/3.00
Mean (log ϵ(V I))	⋯	⋯	2.66 ± 0.14	3.20 ± 0.15	3.03 ± 0.13	2.81 ± 0.12
Cr I λ4708.02[b]	3.17	0.11	68/4.50	⋯	⋯	⋯
Cr I λ4801.05[b]	3.12	−0.13	61/4.51	⋯	74/4.55	79/4.89
Cr I λ4936.34[b]	3.11	−0.34	52/4.54	⋯	70/4.64	⋯
Cr I λ5272.01[b]	3.45	−0.42	40/4.82	63/4.93	53/4.83	23/4.45
Cr I λ5287.20[b]	3.44	−0.90	⋯	49/5.16	33/4.94	⋯
Cr I λ5300.74[b]	0.98	−2.12	116/4.49	160/4.89	137/4.47	113/4.44
Cr I λ5304.18[b]	3.46	−0.68	⋯	53/5.01	27/4.60	24/4.76
Cr I λ5628.62[b]	3.42	−0.77	⋯	⋯	⋯	⋯
Cr I λ5781.16[b]	3.01	−2.15	⋯	⋯	⋯	⋯
Cr I λ6882.48[b]	3.44	−0.38	42/4.70	75/4.94	51/4.61	30/4.48
Cr I λ6883.00[b]	3.44	−0.42	37/4.65	⋯	⋯	26/4.45
Mean (log ϵ(Cr I))	⋯	⋯	4.60 ± 0.13	5.00 ± 0.1	4.66 ± 0.16	4.58 ± 0.20
Mn I λ4671.69[b]	2.89	−1.66	32/4.45	65/4.83	34/4.26	⋯
Mn I λ4709.71[b]	2.89	−0.34	91/4.32	125/4.89	111/4.58	92/4.35
Mn I λ4739.11[b]	2.94	−0.49	⋯	113/4.83	88/4.24	87/4.44
Mn I λ5004.89[b]	2.92	−1.64	31/4.40	⋯	36/4.27	⋯
Mn I λ5388.54[b]	3.37	−1.62	⋯	⋯	26/4.63	⋯
Mean (log ϵ(Mn I))	⋯	⋯	4.39 ± 0.06	4.85 ± 0.04	4.40 ± 0.2	4.40 ± 0.07
Fe I λ6151.61	2.17	−3.28	85/6.12	⋯	120/6.57	⋯
Fe I λ6157.73	4.07	−1.22	81/6.61	⋯	⋯	80/6.61
Fe I λ6165.36	4.14	−1.46	49/6.34	76/6.89	49/6.26	46/6.31
Fe I λ6173.34	2.22	−2.89	114/6.34	146/6.84	129/6.40	⋯
Fe I λ6180.20	2.73	−2.66	96/6.48	⋯	⋯	⋯
Fe I λ6187.99	3.94	−1.67	50/6.29	80/6.88	68/6.53	55/6.42
Fe I λ6200.32	2.61	−2.41	118/6.50	⋯	⋯	108/6.33
Fe I λ6219.28	2.20	−2.42	144/6.41	186/6.99	161/6.49	139/6.35
Fe I λ6226.74	3.88	−2.19	31/6.38	⋯	42/6.48	34/6.47
Fe I λ6229.23	2.84	−2.80	81/6.49	⋯	86/6.40	⋯
Fe I λ6232.64	3.65	−1.23	111/6.64	130/7.00	113/6.55	105/6.53
Fe I λ6246.32	3.60	−0.85	139/6.71	135/6.64	126/6.36	⋯
Fe I λ6252.56	2.40	−1.67	172/6.40	190/6.63	⋯	180/6.57
Fe I λ6265.14	2.18	−2.56	154/6.69	177/6.96	153/6.44	138/6.43
Fe I λ6270.22	2.86	−2.60	99/6.66	⋯	112/6.73	92/6.54
Fe I λ6297.79	2.22	−2.74	⋯	161/6.92	133/6.31	127/6.44
Fe I λ6301.50	3.65	−0.72	132/6.52	152/6.88	141/6.57	⋯
Fe I λ6302.49	3.69	−1.11	99/6.33	135/7.04	117/6.56	100/6.35

Table 2
(Continued)

Wavelength (Å)	χ(eV) (eV)	log gf	LEID 34225 (mÅ)/log $\epsilon(E)$[a]	LEID 39048 (mÅ)/log $\epsilon(E)$[a]	LEID 61067 (mÅ)/log $\epsilon(E)$[a]	LEID 32169 (mÅ)/log $\epsilon(E)$[a]
Fe I λ6311.50	2.83	−3.17	48/6.27	77/6.69	72/6.48	55/6.40
Fe I λ6315.81	4.07	−1.69	57/6.62	76/7.00	56/6.51	65/6.77
Fe I λ6322.69	2.59	−2.41	123/6.54	145/6.86	134/6.55	113/6.37
Fe I λ6335.33	2.20	−2.17	150/6.24	⋯	167/6.31	⋯
Fe I λ6336.83	3.69	−0.85	⋯	153/7.09	120/6.37	115/6.40
Fe I λ6344.15	2.43	−2.92	⋯	126/6.76	⋯	⋯
Mean (log ϵ(Fe I))	⋯	⋯	6.46 ± 0.16	6.88 ± 0.14	6.47 ± 0.12	6.45 ± 0.12
Fe II λ6149.24	3.89	−2.78	26/6.51	⋯	20/6.49	21/6.39
Fe II λ6247.56	3.89	−2.43	35/6.42	⋯	33/6.55	38/6.54
Mean (log ϵ(Fe II))	⋯	⋯	6.46 ± 0.06	⋯	6.52 ± 0.04	6.46 ± 0.11
Co I λ5212.69[b]	3.51	−0.11	⋯	51/4.21	46/4.01	⋯
Co I λ5280.63[b]	3.63	−0.03	36/3.98	60/4.48	33/3.83	20/3.65
Co I λ5301.04[b]	1.71	−2.00	66/3.92	88/4.20	92/4.20	69/4.01
Co I λ5352.04[b]	3.58	0.06	55/4.18	65/4.40	59/4.16	39/3.91
Co I λ5647.23[b]	2.28	−1.56	41/3.78	68/4.18	66/4.03	⋯
Co I λ6093.14[b]	1.74	−2.44	54/4.10	81/4.45	49/3.81	46/4.02
Co I λ6455.00[b]	3.63	−0.25	33/4.07	43/4.30	29/3.90	20/3.81
Mean (log ϵ(Co I))	⋯	⋯	4.01 ± 0.14	4.32 ± 0.13	4.00 ± 0.16	3.88 ± 0.15
Ni I λ5157.98[b]	3.61	−1.51	28/5.20	⋯	42/5.42	28/5.23
Ni I λ5537.11[b]	3.85	−2.20	⋯	⋯	⋯	⋯
Ni I λ6175.37	4.09	−0.55	⋯	58/5.54	44/5.11	36/5.02
Ni I λ6176.81	4.09	−0.42	⋯	70/5.48	54/5.01	43/4.86
Ni I λ6177.25	1.83	−3.53	⋯	⋯	47/4.95	40/5.07
Ni I λ6186.71	4.11	−0.96	⋯	47/5.75	30/5.25	19/5.04
Ni I λ6204.60[b]	4.09	−0.82	25/5.02	43/5.79	⋯	26/5.36
Ni I λ6223.99[b]	4.11	−0.91	⋯	57/5.91	41/5.43	23/5.09
Ni I λ6327.60	1.68	−3.14	⋯	124/5.82	96/5.18	89/5.30
Ni I λ6378.26	4.15	−0.83	28/5.16	46/5.87	41/5.40	40/5.44
Mean (log ϵ(Ni I))	⋯	⋯	5.13 ± 0.09	5.74 ± 0.17	5.22 ± 0.2	5.16 ± 0.2
La II λ6262.29	0.40	−1.22	76/1.10	93/1.32	108/1.46	70/1.03
Mean (log ϵ(La II))	⋯	⋯	1.10	1.32	1.46	1.03

Notes. The table gives the wavelength (Å), lower excitation potential (eV), transition probabilities (log gf), and measured equivalent widths/log $\epsilon(E)$ for that line, for different species.
[a] log $\epsilon(E)$ is the abundance derived for that line.
[b] These lines are from Ramírez & Allende Prieto (2011), and other lines are from Johnson & Pilachowski (2010).

band for its derived stellar parameters: ($T_{\rm eff}$, log g, ξ_t, [Fe/H]) = (4035 ± 50 K, 0.85 ± 0.1, 1.6 ± 0.2, −1.0). The MgH band is synthesized by varying the Mg abundance. The spectrum synthesized for log ϵ(Mg) = 6.85 dex ([Mg/Fe] = +0.25) provides the best fit to the observed spectrum (see Figure 7). The derived Mg abundance from Mg I lines is about 7.0 ± 0.1 ([Mg/Fe] = +0.4). The Mg abundance required for obtaining the best fit for the observed spectrum is 6.85 dex, and this is about 0.15 dex less than that derived from Mg I lines but is in fair agreement within the uncertainties on the derived abundances.

LEID 39048: This is the first-group sample star, which is relatively metal-rich, having strong Mg *b* lines and the MgH band. From the previous study, which contained low-resolution spectroscopic studies of ω Cen giants (Hema & Pandey 2014), this is one of the identified mildly H-deficient stars of our sample, having a very low Mg abundance as expected for its metallicity, as well as from the mean Mg abundance of the ω Cen giants. The Mg abundance was estimated from the MgH band for the star's derived stellar parameters.

In the present study we have used a high-resolution spectrum. The MgH band is synthesized for the star's derived stellar parameters, ($T_{\rm eff}$, log g, ξ_t, [Fe/H]) = (3965 ± 50 K, 0.95 ± 0.1, 1.6 ± 0.2, −0.65), and for the Mg abundance determined from Mg I lines of 7.4 dex ([Mg/Fe] = +0.42). To obtain the best fit for the MgH band, the Mg abundance has to be reduced by about 0.4 dex more than that determined from Mg I lines. This best-fit value of the Mg abundance, derived from the MgH band, is beyond the uncertainty limit on the derived Mg abundance from Mg I lines. Hence, this confirms our 2014 results using a low-resolution spectrum. Figure 8 shows the synthesis for LEID 39048 for the best-fit Mg abundance and also for the derived Mg abundance from Mg I lines, including a different Mg abundance, which do not provide the best fit to the observed MgH band.

The spectrum of the program star LEID 39048 in the MgH band region was synthesized by changing the stellar parameters within the uncertainties that are discussed in Section 3. Our aim was to explore whether the difference in Mg abundance, from Mg I lines and from MgH band, could be accounted for by making changes in the adopted stellar parameters within the uncertainties. The synthesized MgH band for the uncertainties on effective temperature, which are +50 K and −50 K, provides the best fit for the Mg abundance, which is about 0.3 and 0.5 dex lower than the Mg abundance from Mg I lines,

Table 3
List of Fe I and Fe II Lines from Ramírez & Allende Prieto (2011)

Wavelength (Å)	χ (eV)	log gf	LEID 34225 (mÅ)/log $\epsilon(E)$[a]
Fe I λ5295.31	4.42	−1.59	25/6.39
Fe I λ5379.57	3.69	−1.51	92/6.72
Fe I λ5386.33	4.15	−1.67	31/6.26
Fe I λ5441.34	4.31	−1.63	38/6.57
Fe I λ5705.46	4.30	−1.35	37/6.26
Fe I λ5778.45	2.59	−3.44	53/6.34
Fe I λ5793.91	4.22	−1.62	55/6.74
Fe I λ6003.01	3.88	−1.06	95/6.50
Fe I λ6027.05	4.08	−1.09	78/6.43
Fe I λ6056.00	4.73	−0.40	73/6.54
Fe I λ6079.01	4.65	−1.02	38/6.38
Fe I λ6093.64	4.61	−1.30	40/6.64
Fe I λ6096.66	3.98	−1.81	64/6.76
Fe I λ6151.62	2.17	−3.28	85/6.12
Fe I λ6165.36	4.14	−1.46	49/6.34
Fe I λ6187.99	3.94	−1.67	50/6.25
Fe I λ6240.65	2.22	−3.29	102/6.52
Fe I λ6270.22	2.86	−2.60	99/6.60
Fe I λ6705.10	4.61	−0.98	37/6.23
Fe I λ6713.74	4.79	−1.40	24/6.61
Fe I λ6726.67	4.61	−1.03	49/6.47
Fe I λ6810.26	4.61	−0.98	49/6.47
Fe I λ6828.59	4.64	−0.82	51/6.37
Fe I λ6842.69	4.64	−1.22	43/6.62
Fe I λ6843.66	4.55	−0.83	61/6.44
Fe I λ7022.95	4.19	−1.15	59/6.23
Fe I λ7132.99	4.08	−1.65	39/6.23
Mean (log ϵ(Fe I))	⋯	⋯	6.45 ± 0.17
Fe II λ4576.33	2.84	−2.95	77/6.24
Fe II λ4620.51	2.83	−3.21	60/6.47
Fe II λ5234.62	3.22	−2.18	79/6.35
Fe II λ5264.80	3.23	−3.13	46/6.54
Fe II λ5425.26	3.20	−3.22	42/6.52
Fe II λ6432.68	2.89	−3.57	39/6.40
Mean (log ϵ(Fe II))	⋯	⋯	6.49 ± 0.1

Notes. The table gives the wavelength (Å), lower excitation potential (eV), transition probabilities (log gf), and measured equivalent widths/log $\epsilon(E)$ derived for that line in the spectrum of program star LEID 34225.
[a] log $\epsilon(E)$ is the abundance derived for that line.

respectively (see Table 6). Similarly, the MgH band is also synthesized for the uncertainties on the log g value, which are ±0.1. For the log g values −0.1 and +0.1 of the adopted log g, the synthesized MgH band provides the best fit for the Mg abundance, which is about 0.4 and 0.5 dex lower than that derived from the Mg I lines, respectively (see Table 6).

A similar exercise was done with the uncertainties on the microturbulence; the strength of the synthesized MgH band shows no appreciable difference with the change in microturbulence.

LEID 34225: This is a third-group sample star that is relatively metal-rich, having strong Mg *b* lines and the MgH band. From our previous study (Hema & Pandey 2014), which contains low-resolution spectroscopic studies of ω Cen giants, this is one of the mildly H-deficient stars of our sample, giving a much lower Mg abundance than expected for its metallicity and also from the mean Mg abundance of the ω Cen giants. This low Mg abundance was derived by synthesizing the MgH band for the star's adopted stellar parameters using the observed low-resolution spectrum.

A high-resolution spectrum is used in the present study. The MgH band is synthesized for the star's derived stellar parameters, ($T_{\rm eff}$, log g, ξ_t, [Fe/H]) = (4265 ± 50 K, 1.30 ± 0.1, 1.6 ± 0.1, −1.0), and for the Mg abundance determined from Mg I lines of 6.65 ± 0.05 dex ([Mg/Fe] = 0.1). To obtain the best fit to the observed high-resolution spectrum, the Mg abundance has to be reduced by about 0.4 dex more than that derived from Mg I lines. This best-fit value of the Mg abundance is outside the uncertainty limits on the Mg abundance from Mg I lines. Hence, this confirms our 2014 results. Figure 9 shows the synthesis of the MgH band for the best-fit Mg abundance, for the derived Mg abundance from Mg I lines, and also for a lower Mg abundance than that provided by the best fit.

The spectra of the MgH band region were synthesized by changing the stellar parameters within the uncertainties that are discussed in Section 3. Our aim was to explore whether the difference in Mg abundance, from Mg I lines and from MgH band, could be accounted for by making changes in the adopted stellar parameters within the uncertainties. The synthesized MgH band for the uncertainties on effective temperature, which are +50 K and −50 K, provides the best fit for the Mg abundance, which is about 0.3 and 0.5 dex lower than the Mg abundance from Mg I lines, respectively (see Table 6). Similarly, the MgH band is also synthesized for the uncertainties on the log g value, which are ±0.1. For the log g values, −0.1 and +0.1 of the adopted log g, the synthesized MgH band provides the best fit for the Mg abundance, which is about 0.3 dex lower than that derived from the Mg I lines (see Table 6).

A similar exercise was done with the uncertainties on the microturbulence; the strength of the synthesized MgH band shows no appreciable difference with the change in microturbulence.

5. Discussion

The aim of Hema & Pandey (2014) was to identify the H-deficient stars of RCB type, which show a severe H deficiency. The features that directly indicate the H deficiency are H-Balmer lines, CH band, etc. Hβ and CH band were not covered in the observed low-resolution spectra; however, a saturated Hα line is present. Hence, the (0,0) MgH band was used for the analysis. The region of the (0,0) MgH band also includes the strong Mg *b* lines, and these indicate the appropriate metallicity and the Mg abundance of the program stars. The four stars that were identified as H-poor were confirmed by the spectrum synthesis. Though the accurate stellar parameters and the metallicity were available for the program stars, the Mg abundances were not known. In this study, the stellar parameters and the elemental abundances, especially the Mg abundance from Mg I lines, were rederived using the high-resolution spectra of the program stars obtained from SALT-HRS.

In the observed high-resolution spectra, initially we looked for the strengths of the H-Balmer line and the CH band. But the H-Balmer lines in the observed spectra of the program stars are strong and as expected for the stars' stellar parameters. The CH band could not be detected in the spectra of these stars, due to poor signal at about 4300 Å. Hence, the analysis is based on the strength of the (0,0) MgH band in the observed SALT spectra. The two stars are mildly H-poor as expected. According to Hema & Pandey (2014), the third-group sample star LEID 34225 has

Table 4
Derived Abundance Ratios for the Program Stars

Elements	Sun log$\epsilon(E)$	39048[a] [E/Fe]	n[d]	61067[b] [E/Fe]	n[d]	34225[c] [E/Fe]	n[d]	32169[b] [E/Fe]	n[d]
O I	8.69	0.03	2	0.14	1	−0.05	1	0.11	2
Na I	6.24	0.88	2	1.17	4	0.52	4	0.77	4
Mg I	7.60	0.43	5	0.41	5	0.1	4	0.26	4
Mg from MgH	⋯	0.02	⋯	0.26	⋯	−0.28	⋯	0.25	⋯
Al I	6.45	0.67	4	0.92	4	1.09	4	0.75	4
Si I	7.51	0.47	7	0.64	7	0.53	5	0.38	6
Ca I	6.34	0.18	8	0.32	9	0.11	9	0.31	10
Sc I	3.15	⋯	⋯	0.12	6	0.13	4	0.0	3
Sc II	⋯	0.06	5	0.14	7	0.14	5	0.1	5
Ti I	4.95	0.48	11	0.46	17	0.39	7	0.1	14
Ti II	⋯	⋯	⋯	0.46	3	0.39	4	0.1	3
V I	3.93	−0.11	8	0.08	7	−0.23	6	−0.07	8
Cr I	5.64	−0.02	5	0.02	7	0.0	7	0.01	6
Mn I	5.43	0.04	3	−0.02	5	0.01	3	0.02	2
Fe I	7.50	−0.62	16	−1.01	19	−1.05	21	−1.05	16
Fe II	⋯	⋯	⋯	−1.05	2	−1.05	2	−1.06	2
Co I	4.99	−0.06	7	0.02	8	0.05	6	−0.04	5
Ni I	6.22	0.14	7	−0.01	8	−0.06	3	−0.02	9
La II	1.10	0.62	1	1.21	1	1.04	1	1.0	1

Notes. The adopted solar abundances from Asplund et al. (2009) are also given.
[a] First-group H-deficient star.
[b] First-group normal stars.
[c] Third-group H-deficient star.
[d] n is the number of lines used in the analysis.

Table 5
Errors due to the Uncertainties on the Stellar Parameters of LEID 34225, Defined by $\Delta(\log \epsilon_i) = \log \epsilon_i$ (Perturbed)—$\log \epsilon_i$ (Adopted)

Species	$T_{\rm eff} = -50$ (K)	$\log g = -0.1$ (cgs)	$\xi_{\rm turb} = -0.1$ km s^{-1}	Error$_{\rm S/N}$	RMS[a]	SD[b]
O I	−0.04	−0.01	0.03	0.08	0.09	⋯
Na I	−0.06	−0.05	0.01	0.09	0.11	0.16
Mg I	−0.02	−0.005	0.02	0.1	0.10	0.05
Mg(MgH)[c]	⋯	⋯	⋯	0.05	0.05	⋯
Al I	−0.04	0.0	0.025	0.08	0.10	0.12
Si I	0.03	−0.025	0.02	0.09	0.10	0.11
Ca I	−0.08	−0.005	0.04	0.07	0.11	0.16
Sc I	−0.01	−0.04	0.04	0.09	0.10	0.16
Sc II	−0.01	−0.045	0.02	0.08	0.09	0.09
Ti I	−0.1	−0.005	0.035	0.1	0.13	0.14
Ti II	0.01	−0.04	0.07	0.08	0.11	0.11
V I	−0.12	−0.01	0.01	0.09	0.14	0.14
Cr I	−0.07	0.0	0.02	0.09	0.11	0.13
Mn I	−0.07	−0.005	0.015	0.1	0.11	0.06
Fe I	−0.04	−0.025	0.045	0.1	0.12	0.16
Fe II 0.08	−0.055	0.015	0.08	0.13	0.06	
Co I	−0.01	−0.025	0.015	0.09	0.10	0.14
Ni I	−0.06	−0.02	0.015	0.1	0.11	0.1
La I	−0.02	−0.06	0.1	0.09	0.14	⋯

Notes. The adopted parameters are $T_{\rm eff} = 4265$ K, $\log g = 1.3$ (cgs), and $\xi_{\rm turb} = 1.6$ km s^{-1}.
[a] The rms of the error on $T_{\rm eff}$, $\log g$, ξ_t and the error on signal-to-noise ratio of the spectrum.
[b] SD, the standard deviation on the abundance due to the line-to-line scatter.
[c] The error on synthesis due to the error in signal-to-noise ratio is given. Errors due to uncertainties on the stellar parameters for the MgH band are discussed in Table 6.

strong Mg *b* lines and weak/no MgH band. The same traits are observed in the high-resolution spectrum of this star. Also, the first-group sample star LEID 39048, having strong Mg *b* lines and strong MgH band, is also in line with its SALT high-resolution spectrum. The observed MgH band of the program stars was analyzed mainly by spectrum synthesis.

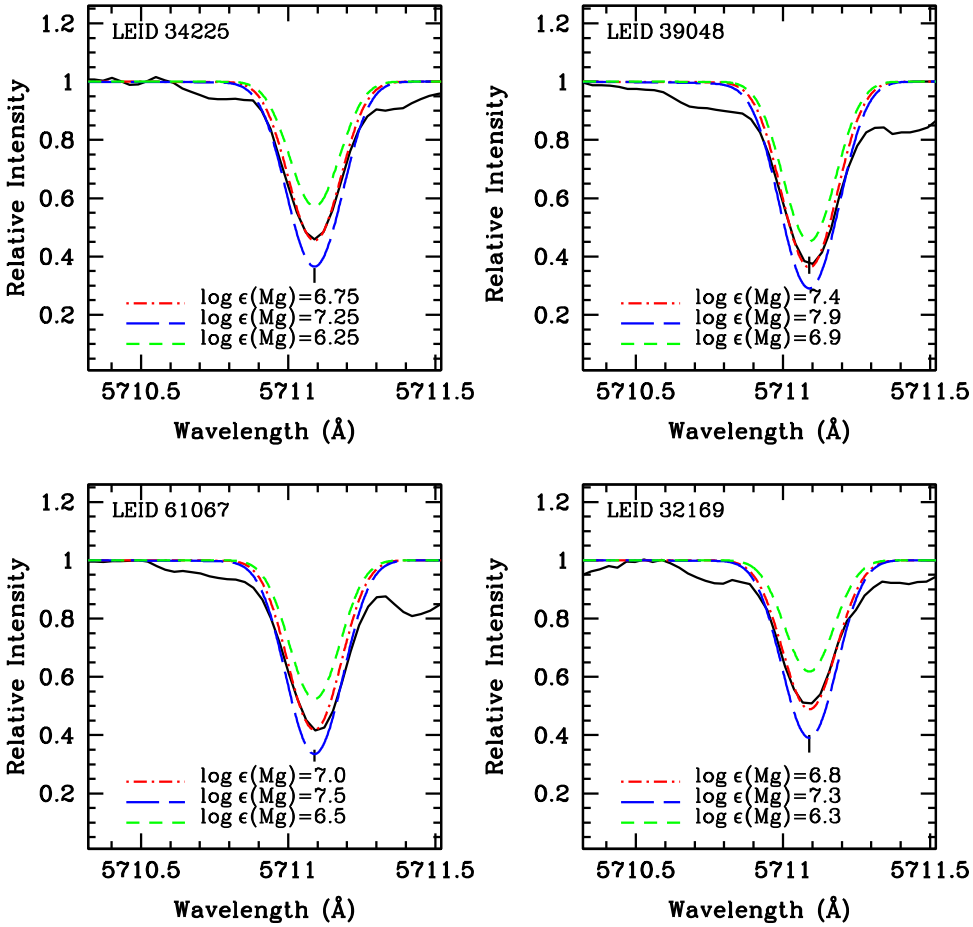

Figure 4. Synthesis of the Mg I line at 5711 Å for the program stars. The synthesis is shown for the best-fit Mg abundance and also for the other two Mg abundances for comparison.

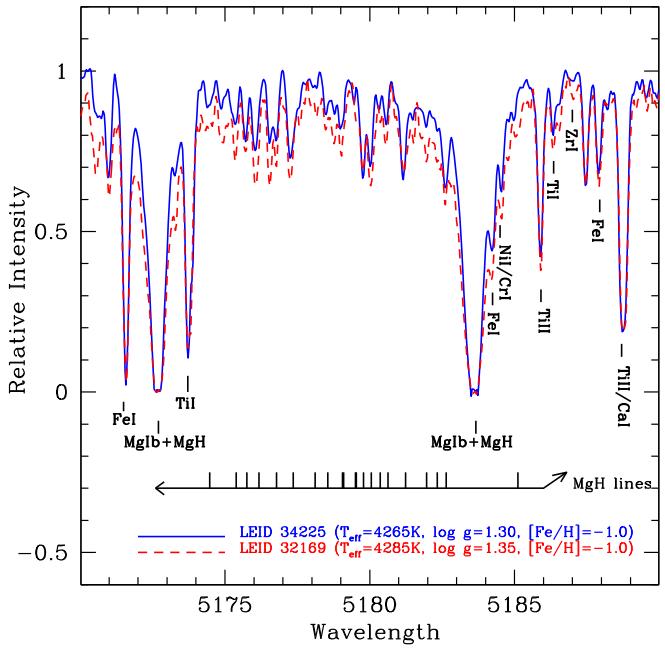

Figure 5. Strengths of the (0,0) MgH band in the spectra of first-group stars LEID 34225 (sample) and LEID 32169 (comparison). The key lines are marked.

For LEID 32169, a normal (H-rich) comparison star, the best fit of the synthesized spectrum of the MgH band, for the star's adopted stellar parameters, to the observed spectrum is obtained for the Mg abundance of 6.8 dex (see Figure 6). The Mg abundances derived from the Mg I lines and the MgH band are in excellent agreement, as expected. Similarly, for LEID 61067, a normal (H-rich) comparison star, the best fit of the synthesized spectrum of the MgH band, for the star's adopted stellar parameters, to the observed spectrum is obtained for the Mg abundance of 6.85 (see Figure 7). This Mg abundance from the MgH band is about 0.15 dex less than the derived Mg abundance from the Mg I lines. This difference in abundance is within the uncertainties, which are about ±0.1 dex on the derived Mg abundance from Mg I lines.

For LEID 39048, a candidate H-deficient star of our sample, the best fit of the synthesized spectrum of the MgH band, for the star's adopted stellar parameters, to the observed spectrum is obtained for the Mg abundance of 7.0 dex ([Mg/Fe] = 0.02 dex; see Figure 8). This Mg abundance is about 0.4 dex less than that derived from the Mg I lines. This difference between the derived Mg abundance from Mg I lines and that from the MgH band is greater than the uncertainty on the Mg abundances from Mg I lines. The spectra were also synthesized by changing the stellar parameters within the uncertainties; the derived Mg abundance from Mg I lines and that from

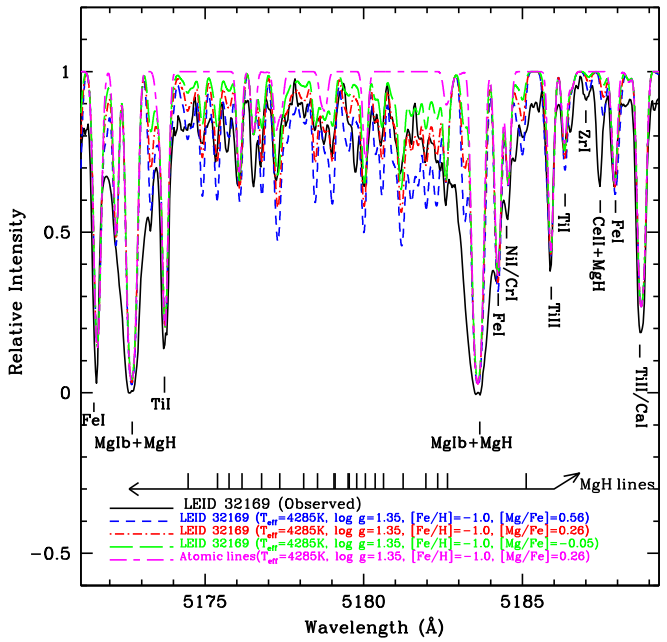

Figure 6. Superposition of the observed and the synthesized spectra for the normal sample star LEID 32169. The spectrum is synthesized for the star's derived stellar parameters and the Mg abundance. The synthesis is shown for the best-fit [Mg I/Fe] = +0.26 with the red dot-dashed line, the synthesis for [Mg/Fe] = +0.56 is shown with the blue short-dashed line, and the synthesis for [Mg/Fe] = −0.05 is shown with the green long-dashed line, for comparison. The synthesis for pure atomic lines is also shown with the magenta short/long-dashed line. The key lines are marked.

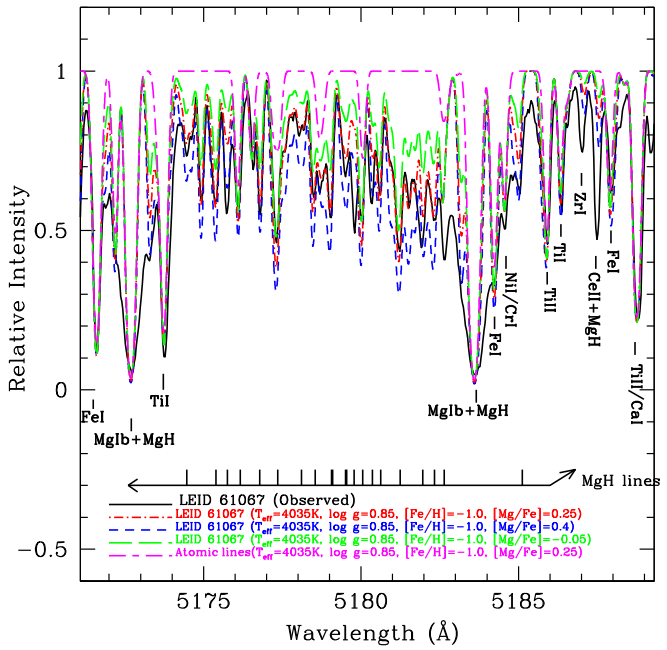

Figure 7. Superposition of the observed and synthesized spectra for the sample star LEID 61067. The spectrum is synthesized for the star's derived stellar parameters and the Mg abundance. The synthesis is shown for [Mg/Fe] = +0.4 with the blue short-dashed line, the best fit [Mg/Fe] = +0.25 with the red dot-dashed line, and also for [Mg/Fe] = −0.05 with the green long-dashed line for comparison. Note that the Mg abundances obtained from Mg I and MgH are in fair agreement within the errors. The synthesis for pure atomic lines is also shown with the magenta short/long-dashed line. The key lines are marked.

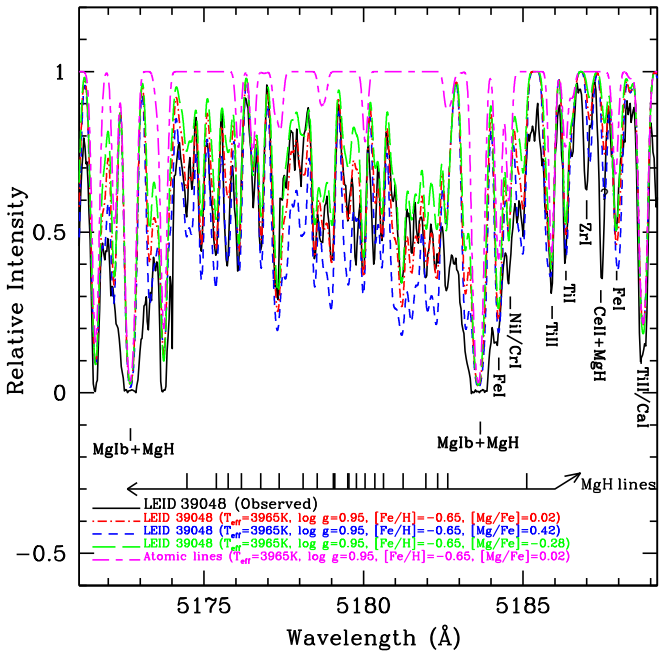

Figure 8. Superposition of the observed and synthesized spectra for the sample star LEID 39048. The spectrum is synthesized for the star's derived stellar parameters and the Mg abundance. The synthesis is shown for [Mg/Fe] = +0.42 from Mg I lines with the blue short-dashed line, the best-fit [Mg/Fe] = +0.02 with the red dot-dashed line, and also for [Mg/Fe] = −0.28 with the green long-dashed line, for comparison. The synthesis for pure atomic lines is also shown with the magenta short/long-dashed line. The key lines are marked.

Table 6
Derived Mg Abundances from Mg I Lines and the MgH Band for the Adopted Stellar Parameters and the Corresponding Uncertainties on Them

Stars	$T_{\rm eff}$	log g	[Mg/Fe] from Mg I	[Mg/Fe] from MgH
LEID 39048	**3965**	**0.95**	**+0.42**	**+0.02**
	4015	0.95	+0.41	+0.11
	3915	0.95	+0.44	−0.06
	3965	1.05	+0.44	−0.08
	3965	0.85	+0.42	+0.02
LEID 34225	**4265**	**1.30**	**+0.10**	**−0.30**
	4315	1.30	+0.10	−0.25
	4215	1.30	+0.06	−0.44
	4265	1.40	+0.04	−0.26
	4265	1.20	+0.06	−0.26

Note. The adopted stellar parameters and their corresponding derived Mg abundances are given in boldface.

the MgH band do not match even within the uncertainties. The Mg abundance required to fit the observed spectrum for the adopted stellar parameters and the uncertainties on them always require an Mg abundance that is lower by about 0.3 dex or more than that derived from the Mg I lines (see Table 6). This difference between the Mg abundances from Mg I lines and the MgH band is not acceptable, as the Mg abundance from Mg I lines and that from the MgH band are expected to be the same within the uncertainties (as seen from the analysis of the spectra of the normal comparison stars—see above).

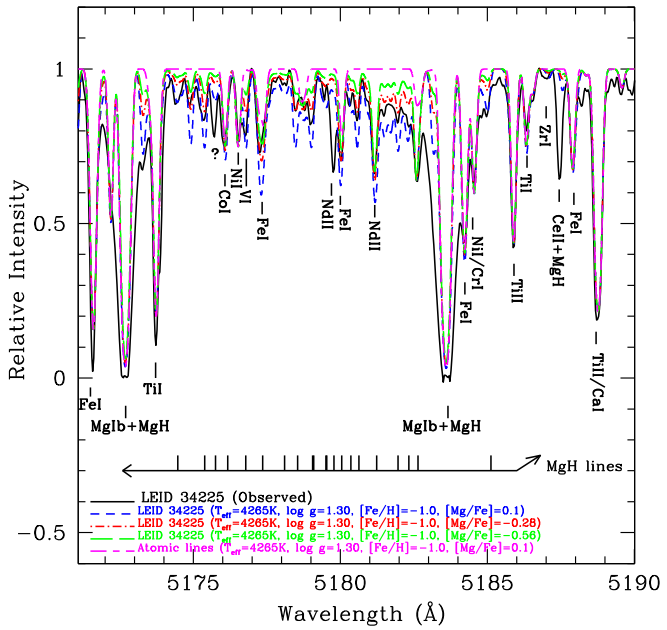

Figure 9. Superposition of the observed and synthesized spectra for the sample star LEID 34225. The spectrum is synthesized for the star's derived stellar parameters and the Mg abundance. The synthesis is shown for [Mg/Fe] = +0.1 from Mg I lines with the blue short-dashed line, for the best-fit [Mg/Fe] of −0.28 with the red dot-dashed line, and also for [Mg/Fe] of −0.56 with the green long-dashed line for comparison. The synthesis for pure atomic lines is also shown with the magenta short/long-dashed line. The key lines are marked.

Similarly, for LEID 34225, another candidate H-deficient star of our sample, the best fit of the synthesized spectrum, for the star's adopted stellar parameters, to the observed spectrum is obtained for the Mg abundance of 6.28 dex ([Mg/Fe] = −0.3) (see Figure 9). This Mg abundance is about 0.4 dex less than that derived from the Mg I lines. The spectra were also synthesized by changing the stellar parameters within the uncertainties. The Mg abundance required to fit the observed spectrum for the adopted stellar parameters and the uncertainties on them always require an Mg abundance that is lower by about 0.3 dex or more than that derived from the Mg I lines (see Table 6). This difference between the Mg abundances from Mg I lines and the MgH band is not acceptable, as the Mg abundance from Mg I lines and that from the MgH band are expected to be same within the uncertainties.

The GGC ω Cen is well known for hosting multiple stellar populations not only in the red giant branch stars but also in the main-sequence (MS) and subgiant branches. Among the red giant stars, about four distinct subpopulations are identified by Calamida et al. (2009): metal-poor ([Fe/H] $\leqslant -1.49$), metal-intermediate ($-1.49 <$ [Fe/H] $\leqslant -0.93$), metal-rich ($-0.95 <$ [Fe/H] $\leqslant -0.15$), and solar metallicity ([Fe/H] ≈ 0). Among the subgiant branch stars, there are about three distinct subpopulations identified by Villanova et al. (2007): SGB-metal-poor ([Fe/H] ~ -1.7), SGB-metal-intermediate ($-1.7 <$ [Fe/H] < -1.4), and SGB-a ([Fe/H] ~ -1.1). Based on the metallicity, two MSs are identified by Piotto et al. (2005): a red MS with ([Fe/H] ~ -1.6), and a blue MS with ([Fe/H] ~ -1.3). There are also multiple stellar population studies in horizontal branch (HB) stars by Tailo et al. (2016). They identify the HB stars as metal-poor ($-2.25 \leqslant$ [Fe/H] $\leqslant -1.4$), metal-intermediate ($-1.4 \leqslant$ [Fe/H] $\leqslant -1.1$), and metal-rich ([Fe/H] $\geqslant -1.1$).

According to these subpopulations, from the MS through SGB and RGB, there is a metal-rich group having a metallicity ([Fe/H] $\sim -1.1 \pm 0.3$), derived spectroscopically, that suggests that they are closely related. From the detailed studies of the MS branches, it is revealed that the bMS stars are helium enriched with an amount $0.35 < Y < 0.45$ and are metal-rich by about 0.3 dex more than the majority of red MS stars, which are He-normal ($Y = 0.28$). However, there are no helium enhancement studies reported for SGB stars, but the SGBs with metallicities similar to the bMS stars are observed. Also, these are identified as the SGB-a group by Villanova et al. (2007). Villanova et al. (2007) have compared their results of the abundance analyses of SGB-a stars with that of the bMS stars from Piotto et al. (2005). The derived abundances, [C/Fe], [N/Fe], and [Ba/Fe], for bMS stars and SGB-a are very similar, ascertaining the connection between these groups. Pancino et al. (2011) have studied metal-rich subgiants for determining their lithium abundance along with the α-peak elements, [Al/Fe] and [Ba/Fe]. These abundance ratios, [α/Fe], [Al/Fe], and [Ba/Fe], for their sample are in agreement with the literature. They suspect that all the H-burning processes, where He is produced, happen at temperatures where Li is destroyed. Therefore, He-rich stars should have a very low lithium content. In their sample, they have found a lithium abundance that is lower than that expected for these metal-rich subgiants (see Pancino et al. 2011, for details). Hence, it is an indirect clue that the metal-rich subgiant stars are He-rich.

In connection with evolution of the metal-rich stars, our program stars provide a further link to this evolutionary track. Our program stars are metal-rich with a metallicity [Fe/H] $\geqslant -1.1$. Using the high-resolution spectra, a detailed abundance analysis is carried out. In order to check the similarities of our program stars to the metal-rich stars of MS:bMS and SGB:SGB-a, we compared their elemental abundances. Mainly the α- and Fe-peak elements are compared, as these remain unaltered in the course of the evolution of these stars. The elemental abundances determined for the program stars agree within $\pm$0.2 dex with those derived by Johnson & Pilachowski (2010). This uncertainty arises because the spectra used are obtained from different instruments with different resolution. The solar-scaled elemental abundances plotted versus metallicity for the program stars are shown in Figures 10–12. The abundance ratios from Johnson & Pilachowski (2010) are shown with filled circles. Johnson & Pilachowski (2010) have adopted the solar abundances from Anders & Grevesse (1989), and we have adopted the solar abundances from Asplund et al. (2009); differences due to the adopted solar abundances are taken into account. The α-processed elements, such as Mg, Si, and Ca, show enhancement by about 0.2–0.7 dex, which is in fair agreement with those derived by Johnson & Pilachowski (2010) for the metal-rich RGB stars of ω Cen (see Figure 10). [Na/Fe] shows enhancement of about 0.5–1.2 dex for the program stars, which is as expected for the metal-rich stars from Johnson & Pilachowski (2010) (see Figure 10). [Ti/Fe] shows an enhancement on an average of 0.35 dex for the program stars (see Figure 11). Johnson & Pilachowski (2010) find that for the metal-rich RGBs [Ti/Fe] $\approx$ 0.3 dex. The Fe-peak elements, such as Cr, Mn, Co, and Ni, do not show any enhancement (see Figure 12). Johnson & Pilachowski (2010) have given abundances of Ni for the RGBs that are in good agreement with those of our program stars.

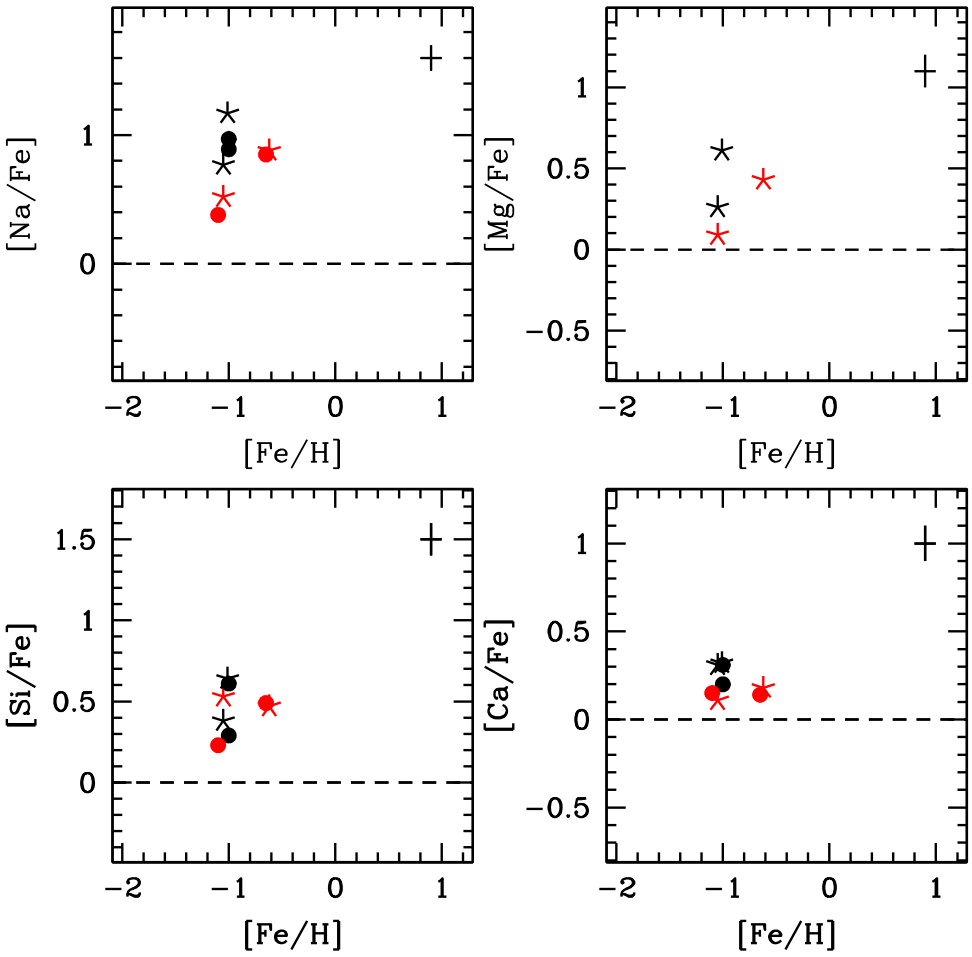

Figure 10. Abundance ratios with respect to solar vs. metallicity for the program stars. The red stars are the mildly H-deficient stars, and the black stars are the normal comparison stars. The filled circles represent the elemental abundances derived by Johnson & Pilachowski (2010) for the program stars, the red circles the mildly H-deficient/He-enhanced stars, and the black circles the normal (H-rich) stars. The horizontal dotted lines show the solar-scaled abundance values. The error bars on the abundance ratios are shown with crossed thick lines in the upper right corner.

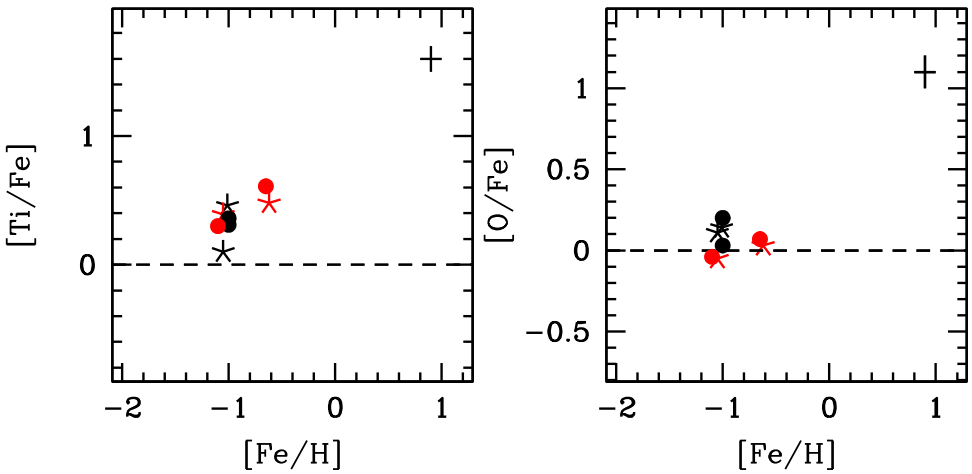

Figure 11. Abundance ratios with respect to solar vs. metallicity for the program stars. The red stars are the mildly H-deficient stars, and the black stars are the normal comparison stars. The filled circles represent the elemental abundances derived by Johnson & Pilachowski (2010) for the program stars, the red circles the mildly H-deficient/He-enhanced stars, and the black circles the normal (H-rich) stars. The horizontal dotted lines show the solar-scaled abundance values. The error bars on the abundance ratios are shown with crossed thick lines in the upper right corner.

However, [O/Fe] for our program stars are similar to solar and do not show any depletion/enhancement, and they are also similar to [O/Fe] ≈ -0.15 (see Figure 11) for metal-rich RGBs derived by Johnson & Pilachowski (2010). Marino et al. (2011) have conducted high-resolution spectroscopic studies for red giant stars of ω Cen for deriving Fe, Na, O, and n-capture elements. They have studied the Na−O anticorrelation for the giants of different metallicity. The giants in the metal-rich regime do not show any

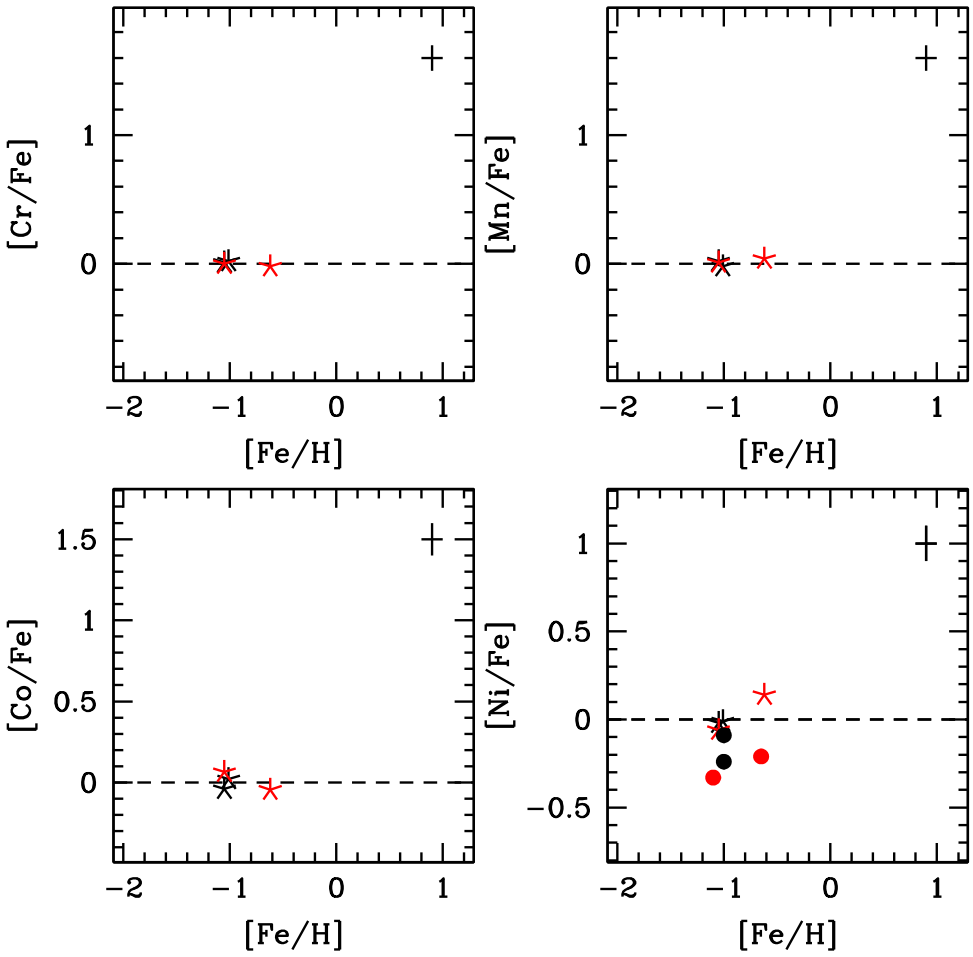

Figure 12. Abundance ratios with respect to solar vs. metallicity for the program stars. The red stars are the mildly H-deficient stars, and the black stars are the normal comparison stars. The filled circles represent the elemental abundances derived by Johnson & Pilachowski (2010) for the program stars, the red circles the mildly H-deficient/He-enhanced stars, and the black circles the normal (H-rich) stars. The horizontal dotted lines show the solar-scaled abundance values. The error bars on the abundance ratios are shown with crossed thick lines in the upper right corner.

Na−O anticorrelation, unlike metal-poor and metal-intermediate giants. This is also observed in our program stars. Lanthanum abundance derived for our program stars is from a single line and is in line with the [La/Fe] versus [Fe/H] plots given by Johnson & Pilachowski (2010), Marino et al. (2011, 2012), and D'Orazi et al. (2011).

For the SGB-a stars, Villanova et al. (2007) have derived the abundances for Ca and for Ti along with C, N, and Ba. The enhancements [Ca/Fe] and [Ti/Fe] of 0.48 and 0.44 dex, respectively, for SGB-a stars by Villanova et al. (2007) are in good agreement with the enhancements [Ca/Fe] and [Ti/Fe] of 0.35 and 0.3 dex, respectively, for our program stars. Similarly, Pancino et al. (2011) have determined $[\alpha/\mathrm{Fe}] = +0.4$ dex, $[\mathrm{Al/Fe}] = +0.32$ dex, and [Fe-peak/Fe] ~ 0.0 dex, which are in excellent agreement with those determined by Villanova et al. (2007) and also those determined for metal-rich giants by Johnson & Pilachowski (2010) and in this study. These abundance similarities link the SGB-a stars to the metal-rich RGB stars of ω Cen.

A very important link between bMS, SGB-a, and metal-rich RGBs comes from the helium enhancement. An unacceptable Mg abundance derived for our sample stars LEID 39048 and LEID 34225, from the MgH bands (the weaker MgH bands), lower than that expected for their derived stellar parameters, and the Mg abundances from Mg I lines and the uncertainties on these parameters suggest the lower hydrogen/He enhancement in their atmospheres.

Hence, similar to bMS stars, our sample stars, which are metal-rich RGBs, show mild deficiency in hydrogen or enhanced helium. All metal-rich RGBs may not be H-poor/He-enhanced, but a subgroup of them are. Dupree et al. (2011) have reported the first direct evidence for an enhancement of helium in the metal-poor RGBs of ω Cen by analyzing the near-infrared He I λ10830 transition in about 12 red giants. From their studies they notice that the He-enhanced giants show enhanced [Al/Fe] and [Na/Fe] over the He-normal giants (see their Figure 10). Figure 13 shows the plot [Al/Fe] versus [Na/Fe] for our program stars along with the Dupree et al. (2011) sample stars. Our program stars follow a similar trend to that of the Dupree et al. (2011) sample stars.

Detailed spectroscopic studies are not available for horizontal branch stars. However, the helium enhancement in horizontal branch stars may also be due to helium-flash or any other processes and may not be wholly intrinsic (Moehler et al. 2002).

6. Conclusions

This study, based on the evaluation of the strengths of the MgH bands in the observed high-resolution spectra and for the

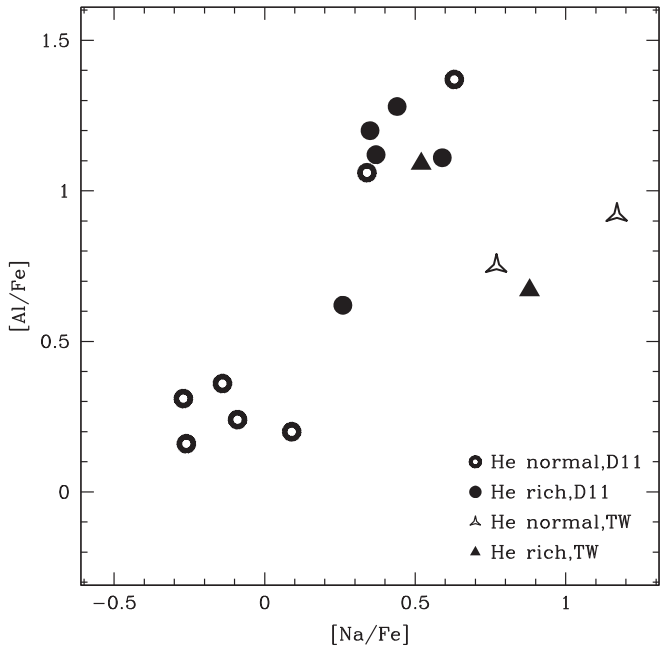

Figure 13. Abundance ratios of [Al/Fe] vs. [Na/Fe]. The open and filled circles are He-normal and He-enhanced giants, respectively, from Dupree et al. (2011), and the open and filled triangles are the He-normal and He-enhanced giants, respectively, from this work (TW).

stars' adopted stellar parameters, confirms that LEID 39048 and LEID 34225 are mildly H-deficient/He-enhanced. Discovery and the detailed abundance analysis of these stars provide direct evidence for the presence of He-enhanced metal-rich giants in ω Cen. These stars provide a crucial link to the evolution of the metal-rich subpopulation of MS, subgiant, and red giant stars.

All of the observations reported in this paper were obtained with the Southern African Large Telescope (SALT). We thank the anonymous referee for a constructive report that improved the presentation of this paper.

ORCID iDs

Gajendra Pandey https://orcid.org/0000-0001-5812-1516

References

Alonso, A., Arribas, S., & Martínez-Roger, C. 1999, A&AS, 140, 261
Anders, E., & Grevesse, N. 1989, GeCoA, 53, 197
Asplund, M., Grevesse, N., Sauval, A. J., & Scott, P. 2009, ARA&A, 47, 481
Bedin, L. R., Piotto, G., Anderson, J., et al. 2004, ApJ, 605, L125
Calamida, A., Bono, G., Stetson, P. B., et al. 2009, ApJ, 706, 1277
Da Costa, G. S., Norris, J. E., & Yong, D. 2013, ApJ, 769, 8
D'Orazi, V., Gratton, R. G., Pancino, E., et al. 2011, A&A, 534, A29
Dupree, A. K., & Avrett, E. H. 2013, ApJL, 773, L28
Dupree, A. K., Strader, J., & Smith, G. H. 2011, ApJ, 728, 155
Hema, B. P., & Pandey, G. 2014, ApJL, 792, L28
Hinkle, K., Wallace, L., Valenti, J., & Harmer, D. 2000, Visible and Near Infrared Atlas of the Arcturus Spectrum 3727-9300 A
Johnson, C. I., & Pilachowski, C. A. 2010, ApJ, 722, 1373
Kurucz, R. L. 1998, http://kurucz.harvard.edu/
Marino, A. F., Milone, A. P., Piotto, G., et al. 2011, ApJ, 731, 64
Marino, A. F., Milone, A. P., Piotto, G., et al. 2012, ApJ, 746, 14
Mayor, M., Meylan, G., Udry, S., et al. 1997, AJ, 114, 1087
McWilliam, A., & Lambert, D. L. 1988, MNRAS, 230, 573
Moehler, S., Sweigart, A. V., Landsman, W. B., & Dreizler, S. 2002, A&A, 395, 37
Pancino, E., Mucciarelli, A., Bonifacio, P., Monaco, L., & Sbordone, L. 2011, A&A, 534, A53
Pandey, G., Lambert, D. L., Rao, N. K., et al. 2004, MNRAS, 353, 143
Piotto, G., Villanova, S., Bedin, L. R., et al. 2005, ApJ, 621, 777
Ramírez, I., & Allende Prieto, C. 2011, ApJ, 743, 135
Simpson, J. D., & Cottrell, P. L. 2013, MNRAS, 433, 1892
Sneden, C. A. 1973, PhD thesis, The Univ. Texas
Sollima, A., Ferraro, F. R., Pancino, E., & Bellazzini, M. 2005, MNRAS, 357, 265
Sumangala Rao, S., Pandey, G., Lambert, D. L., & Giridhar, S. 2011, ApJL, 737, L7
Tailo, M., Di Criscienzo, M., D'Antona, F., Caloi, V., & Ventura, P. 2016, MNRAS, 457, 4525
Villanova, S., Piotto, G., King, I. R., et al. 2007, ApJ, 663, 296